

X-ray Bloch waves in a crystal with a dislocation

V. L. Indenbom, V. M. Kaganer, and É. V. Suvorov

Institute of Crystallography, Academy of Sciences of the USSR; Institute of Solid State Physics, Academy of Sciences of the USSR

(Submitted 28 June 1983)

Zh. Eksp. Teor. Fiz. **86**, 675–690 (February 1984)

The propagation, refraction, and diffraction of x-ray Bloch waves in the strain field of a dislocation are analyzed. If the strain field varies slowly, it is sufficient to consider the curvature of trajectories and the change in the phases of the Bloch waves (the geometric optics of Bloch waves), but when the strain field changes rapidly it becomes necessary to take into account the creation of new Bloch waves (the diffraction optics of Bloch waves). Analysis of the creation of Bloch waves during interbranch scattering in both weak and strong distortion fields makes it possible to construct a Riemann function (influence function) for a crystal with a dislocation. This description of ray and diffraction effects in the optics of Bloch waves is supported by the good agreement of the calculated results with x-ray topographic sections, which directly convey the Riemann function, and also with the results of a numerical simulation of the wave fields.

As it penetrates into a crystal, an x-ray electromagnetic wave undergoes a qualitative change in nature and can be described as a set of Bloch waves corresponding to quasiparticles with a mass whose magnitude and sign depend on the position of the excitation point on the dispersion surface. The behavior of x-ray Bloch waves in ideal crystals has been studied quite thoroughly (see Refs. 1–3, for example). The splitting of the dispersion surface at the boundaries of the Brillouin zone has been studied. An interference of Bloch waves corresponding to the same or different branches of the dispersion surface has been predicted and observed. The corresponding Riemann functions (influence functions) have been constructed, and the problem of the diffraction of bounded and modulated wave packets in ideal crystals has been solved completely. Various methods for using crystals to arrange geometric and diffractive focusing of Bloch waves have been proposed and implemented. An active research program is under way to develop coherent focusing x-ray optics.

In a crystal whose ideal periodicity has been disrupted (by the strain field of a defect, for example) Bloch waves are no longer eigenfunctions of the wave equations. A natural generalization can be made by introducing a local dispersion surface in the region of the crystal of interest: The Bloch waves adjust to the local deviations in the crystal lattice, and their trajectories become curved (the geometric optics of quasiparticles). This approximation is valid when the distortions of the crystal vary smoothly; the pertinent characteristic length here is not the wavelength λ but the extinction length A , which is determined by the splitting of the dispersion surface at the boundary of the Brillouin zone and which is several tens of microns. Although the geometric (ray) optics of Bloch waves is analogous to the optics of media which have a smoothly varying refractive index, the equations of the geometric optics of Bloch waves, in contrast with ordinary optics, describe two families of quasiparticles with rest masses of opposite signs.^{1,2,4} A sharp change in the strain field, to which the Bloch waves cannot adjust, results in a diffraction of these waves, in particular, interbranch scatter-

ing. Each Bloch wave generates an entire family of Bloch waves, and this generation frequently complicates even a qualitative analysis of the scattering mechanisms. The problem of interbranch scattering has been solved exactly only for two-crystal arrangements,⁵ for a uniformly bent crystal,⁶ and in the limit of a δ -shaped change in the distortion, which corresponds to a stacking fault in a crystal.⁷ In the latter case the problem reduces to a re-expansion of the waves in the eigenfunctions of the second part of the crystal, which differs because of the lattice displacement.

As in ordinary optics, it is considerably simpler to analyze the propagation and diffraction of Bloch waves in a medium whose inhomogeneity is of a layered nature, and the strain field varies only over depth in each scattering plane. The coordinate x is cyclic along the reflection vector, and the generalized momentum $P = P_x$ is conserved along the trajectory of a Bloch wave. The geometric-optics equations can accordingly be integrated.⁸ The momentum conservation also simplifies the analysis of the diffraction of the quasiparticles, since now each Bloch wave can undergo interbranch scattering, during which the transverse component of the quasimomentum is conserved; i.e., each Bloch wave can generate only a single new Bloch wave, and this new wave will have the same generalized momentum but will belong to a different sheet of the dispersion surface. The direction of the ray velocity (the group velocity) may change by an angle on the order of the Bragg angle. In the present paper we study the diffraction of Bloch waves in the strain field of a dislocation parallel to the reflection vector. This problem is translationally invariant along the direction of the reflection vector, and we deal with the limiting case of a smooth change in the strain field, the limiting case of a δ -shaped change, and all intermediate cases, depending on the distance between the dislocation and the scattering plane. The same x-ray image can be used to analyze different ray and diffraction mechanisms for image formation.

In Section 1 we derive equations for the amplitudes of the Bloch waves and use the results to analyze the range of applicability of the geometric optics of Bloch waves. In Sec-

tion 2 we identify the regions in which Bloch waves propagate freely and the regions in which they interact (interbranch scattering), and we show that interbranch scattering reduces to a change in the complex amplitudes of the Bloch waves. A perturbation theory is constructed for determining these amplitudes. Section 3 is a detailed analysis of the case of a strong distortion field, to which perturbation theory is not applicable. The diffraction of the Bloch waves is seen most clearly in this case, and the conclusions regarding the mechanisms for image formation and the calculated results can be compared definitively with experiment. In Section 4 we construct a Riemann function for a crystal with a dislocation to describe the propagation of a perturbation from a point source. With decreasing distance from the dislocation to the scattering plane, the free propagation of Bloch waves gives way to a diffraction of the Bloch waves and then to a diffractive focusing of the Bloch waves by the strain field of the dislocation. The trajectories, amplitudes, and phases of the Bloch waves propagating in a crystal are determined; these properties are also determined for the new family of Bloch waves created in the course of interbranch scattering. Section 5 describes the formation of interference images on x-ray topographic sections, which directly convey the Riemann function of a crystal with a dislocation. The phases of the Bloch waves created in the course of interbranch scattering are recorded on these interference images. The reference waves are Bloch waves which have not undergone diffraction. The experimental topographic sections and the results of numerical simulations agree well with calculations on the interference of Bloch waves of different families, showing that the image-formation mechanisms have been determined correctly and that the amplitudes and phases of the Bloch waves have been calculated correctly.

1. X-RAY BLOCH WAVES

X rays interact only very weakly with a medium, since the polarizability in the x-ray range is on the order of 10^{-5} – 10^{-6} . During the diffraction of x rays in a crystal, the amplitude of the diffracted wave thus becomes comparable to that of the incident wave only after the wave has traversed 10^5 – 10^6 coherently scattering atomic layers (i.e., only after the wave has propagated several tens of microns). For thicker perfect crystals, the diffraction can no longer be described in the kinematic approximation (by perturbation theory).⁹ The wave field in a crystal in a reflecting position must be sought as the coherent superposition of transmitted and diffracted waves (see Ref. 1, for example):

$$E = E_0(\mathbf{r}) e^{2\pi i \mathbf{k}_1 \mathbf{r}} + E_1(\mathbf{r}) e^{2\pi i (\mathbf{k}_1 + \mathbf{g}) \mathbf{r}}, \quad (1)$$

where E_0 and E_1 are the slowly varying amplitudes of the transmitted and diffracted waves, respectively, \mathbf{k}_1 is the wave vector of the incident wave, which satisfies the Bragg condition exactly, and \mathbf{g} is the diffraction vector. From Maxwell's equations we find coupled-oscillation equations for the amplitudes E_0 and E_1 : The change in the amplitude of the transmitted wave along its propagation direction is determined by the circumstance that this wave creates a diffracted wave, and vice versa,

$$(\mathbf{k}_1, \nabla) E_0 = i\pi k^2 \chi_{-1} C E_1, \quad (\mathbf{k}_1 + \mathbf{g}, \nabla) E_1 = i\pi k^2 \chi_1 C E_0. \quad (2)$$

Here χ_1 and χ_{-1} are the Fourier components of the polarizability of the crystal for the reflection vectors \mathbf{g} and $-\mathbf{g}$, respectively; $C = 1$ for the σ polarization and $C = \cos 2\theta$ for the π polarization; θ is the Bragg angle; and $k = |\mathbf{k}_1| = |\mathbf{k}_1 + \mathbf{g}|$. The characteristic scattering length in this problem is the extinction length $\Lambda = \cos \theta / Ck (\chi_1 \chi_{-1})^{1/2}$. In an absorbing crystal, the polarizability χ and thus Λ are complex; here $\text{Im } \Lambda \ll \text{Re } \Lambda$. Because of the small x-ray polarizability of the crystal, the extinction length Λ is several tens of microns, justifying the approximation of slowly varying wave amplitudes E_0 and E_1 .

Linearly independent solutions of system (2) correspond to Bloch waves. When we speak in terms of Bloch waves, there will be no scattering of any sort in an ideal crystal, and the extinction-modulation effect corresponds to simply an interference of Bloch waves with different wave vectors, with the difference being on the order of Λ^{-1} .

An incident plane wave of unit amplitude whose wave vector \mathbf{k} differs in direction from \mathbf{k}_1 determines the boundary conditions at the entrance surface of the crystal, $z = -a$:

$$E_0(\mathbf{r})|_{z=-a} = e^{2\pi i (\mathbf{k} - \mathbf{k}_1) \mathbf{r}}, \quad E_1(\mathbf{r})|_{z=-a} = 0. \quad (3)$$

It is convenient to write

$$2\pi (\mathbf{k} - \mathbf{k}_1) \mathbf{r} = \pi \Lambda'^{-1} P x \text{ctg } \theta,$$

where $\Lambda' = \text{Re } \Lambda$, and to thereby convert to expressing the angular deviations in terms of the dynamic units P (a deviation of the incident wave by an angle φ corresponds to $P = 2\Lambda' \lambda^{-1} \varphi \sin \theta$, while the values $P = \pm 1$ correspond to the edges of the ideal Bragg reflection curve).

In a real crystal the polarizability $\chi(\mathbf{r})$ (not averaged over a volume element which is infinitesimally small from the physical standpoint; see Ref. 9) ceases to be a strictly periodic function of the coordinates and depends on the displacement field $\mathbf{u}(\mathbf{r})$. Since the inner electron shells which are responsible for the scattering of the x rays are displaced along with the corresponding nuclei, a change in the polarizability reduces to a replacement of $\chi(\mathbf{r})$ by $\chi[\mathbf{r} - \mathbf{u}(\mathbf{r})]$. The Fourier components of the polarizability, χ_g , become $\chi_g e^{-2\pi i \mathbf{g} \mathbf{u}}$, and corresponding phase factors appear in the coefficients in Eqs. (2) (see Ref. 1, for example). Since we are dealing with displacement fields $\mathbf{u}(\mathbf{r})$ which do not depend along the coordinate (x) in the direction of the diffraction vector \mathbf{g} , the substitution

$$E_0 \rightarrow E_0 \exp\left(i \frac{\pi}{\Lambda'} P x \text{ctg } \theta + i\pi \mathbf{g} \mathbf{u}\right),$$

$$E_1 \rightarrow \left(\frac{\chi_1'}{\chi_{-1}}\right)^{1/2} E_1 \exp\left(i \frac{\pi}{\Lambda'} P x \text{ctg } \theta - i\pi \mathbf{g} \mathbf{u}\right)$$

reduces these equations to a system of ordinary differential equations

$$\frac{d}{dz} \begin{pmatrix} E_0 \\ E_1 \end{pmatrix} = -i \frac{\pi}{\Lambda} \begin{pmatrix} -w & 1 \\ 1 & w \end{pmatrix} \begin{pmatrix} E_0 \\ E_1 \end{pmatrix} \quad (4)$$

with the boundary conditions

$$\begin{pmatrix} E_0 \\ E_1 \end{pmatrix}_{z=-a} = \begin{pmatrix} 1 \\ 0 \end{pmatrix}. \quad (5)$$

Here

$$w = \frac{\Lambda}{\Lambda'} [P - \beta(z)], \quad \beta(z) = \Lambda' \frac{dgu}{dz}. \quad (6)$$

The parameter P describes the deviation of the incident plane wave from satisfaction of the Bragg condition, $\beta(z)$ is the local deviation of the crystal from the Bragg condition, caused by the displacement field $u(\mathbf{r})$, and w is the effective disorientation of the crystal.

Let us examine the symmetry properties of system (4). In the absence of absorption, the quantity w is real. Eliminating E_0 , we find $E_1(z; P, y) = -E_1^*(z; -P, -y)$ from the equation for the wave E_1 and the boundary conditions (here the asterisk means complex conjugation). If, on the other hand, $\beta(z)$ is symmetric with respect to the median plane of the crystal ($z = 0$), i.e., if $\beta(z) = \beta(-z)$, then we would have $E_1(a; P, y) = E_1(a; -P, -y)$ even in the case with absorption (cf. Ref. 10).

Dynamic diffraction involves a mutual scattering of the waves E_0 and E_1 , according to (4). In an undistorted crystal with $w = \text{const}$, it is a simple matter to construct two linearly independent eigensolutions of system (4), i.e., Bloch waves, and to find a linear combination of these waves which satisfies boundary conditions (5). If the disorientation varies slowly, on the other hand (the specific condition will be found below), a natural generalization would consist of modified Bloch waves which interact only weakly in the distorted crystal because of the small value of dw/dz (the quasi-particles begin to interact, but they retain their individuality). At this point we use the linear transformation of Ref. 11, which diagonalizes the matrix of system (4) under the condition $w = \text{const}$:

$$\begin{pmatrix} E_0 \\ E_1 \end{pmatrix} = \hat{B} \begin{pmatrix} \varphi_1 \\ \varphi_2 \end{pmatrix}; \quad \hat{B} = \begin{pmatrix} \Gamma_- & -\Gamma_+ \\ \Gamma_+ & \Gamma_- \end{pmatrix}, \quad (7)$$

$$\Gamma_{\pm} = \left(\frac{1}{2} \left(1 \pm \frac{w}{\gamma} \right) \right)^{1/2}, \quad \gamma = (1+w^2)^{1/2}.$$

We can then transform to equations for the Bloch waves φ_1 and φ_2 :

$$\begin{aligned} \frac{d}{dz} \begin{pmatrix} \varphi_1 \\ \varphi_2 \end{pmatrix} &= -i \frac{\pi}{\Lambda} \begin{pmatrix} \gamma & 0 \\ 0 & -\gamma \end{pmatrix} \begin{pmatrix} \varphi_1 \\ \varphi_2 \end{pmatrix} \\ &+ \frac{w'}{2\gamma^2} \begin{pmatrix} 0 & 1 \\ -1 & 0 \end{pmatrix} \begin{pmatrix} \varphi_1 \\ \varphi_2 \end{pmatrix}, \end{aligned} \quad (8)$$

where $w' = dw/dz$. The first term on the right side of (8) describes the change in the phase of each of the Bloch waves, while the second term describes the interaction of these waves. Ignoring the interaction of the Bloch waves corresponds to adopting the eikonal approximation of the theory of the electron-microscope image¹¹:

$$E_0 = \Gamma_+(-a) \Gamma_+(z) \exp[i\Phi(z)] + \Gamma_-(-a) \Gamma_-(z) \exp[-i\Phi(z)], \quad (9')$$

$$E_1 = -\Gamma_+(-a) \Gamma_-(z) \exp[i\Phi(z)] + \Gamma_-(-a) \Gamma_+(z) \exp[-i\Phi(z)], \quad (9'')$$

where the phase is given by

$$\Phi(z) = \frac{\pi}{\Lambda} \int_{-a}^z (1+w^2)^{1/2} dz. \quad (10)$$

In this approximation the Bloch-wave amplitudes $|\varphi_1|$ and $|\varphi_2|$ are constant. Because of the change in the local disorientation of the crystal, w , the excitation points are displaced along the dispersion surface. As a result, there are changes in the directions of the Poynting vectors; the direction of the trajectories of the quasi-particles changes; and there are corresponding changes in the wave amplitudes E_0 and E_1 in each Bloch wave. In Eqs. (9), these changes are described by the factors $\Gamma_{\pm}(z)$.

2. INTERBRANCH SCATTERING OF BLOCH WAVES

Approximation (9) can of course be derived by the standard method as a semiclassical approximation for Eqs. (4). Our approach has the advantage that the factor $w'/2\gamma^2$ is singled out immediately in (8); this factor determines the interaction of the Bloch waves (interbranch scattering). Ordinarily, the eikonal approximation can be applied to dynamic-diffraction problems only if the change in the disorientation of the crystal is smooth: $\Lambda |\beta'| \ll 1$ (cf. Ref. 12, for example). According to (8), the eikonal approximation is also applicable when a sharp change in the disorientation occurs in a highly disoriented region, with $w \gg 1$; in this region of the crystal the eikonal approximation may be valid for some of the Bloch waves, with certain values of P , for which the disorientation w is large enough.

The quantity $w'/2\gamma^2$ is large only in comparatively small regions of the crystal. In these regions there is a mutual scattering of Bloch waves. Since these regions are small the scattering of the Bloch waves can be described in terms of scattering amplitudes and phase shifts, so that the subsequent propagation of the Bloch waves can be treated in the eikonal approximation, (9), but with altered amplitudes. If the interbranch scattering is not strong, the second term in (8) can be treated as a perturbation. In first-order perturbation theory we can then determine the scattering from the wave φ_1 into φ_2 and the inverse scattering, while in second order we can determine the changes in the amplitudes of each wave. Within this accuracy we can write

$$\begin{pmatrix} \varphi_1(z) \\ \varphi_2(z) \end{pmatrix} = \begin{pmatrix} (1-J_2)e^{-i\Phi} & J_1 e^{-i\Phi} \\ -J_1 e^{i\Phi} & (1-J_2)e^{i\Phi} \end{pmatrix} \begin{pmatrix} \varphi_1(-a) \\ \varphi_2(-a) \end{pmatrix}, \quad (11)$$

where

$$\begin{aligned} J_1 &= \int_{-a}^z dz' \frac{w'(z')}{2\gamma^2(z')} e^{2i\Phi(z')}, \\ J_2 &= \int_{-a}^z dz' \frac{w'(z')}{2\gamma^2(z')} e^{2i\Phi(z')} \int_{-a}^{z'} dz'' \frac{w'(z'')}{2\gamma^2(z'')} e^{-2i\Phi(z'')}, \end{aligned}$$

and the expressions for \tilde{J}_1 and \tilde{J}_2 differ in that i is replaced by $-i$ (this procedure does not reduce to a complex conjugation, since the extinction length Λ is complex in an absorbing crystal).

The interbranch scattering of Bloch waves can be seen most clearly under conditions of strong absorption. Under such conditions, the two Bloch waves in (9) have different

absorption coefficients; to determine these coefficients it is sufficient to consider the imaginary part of the phase $\Phi(z)$ ($\text{Im } \Lambda > 0$, so that $\text{Im } \Phi < 0$). The amplitudes of the Bloch waves decrease in proportion to the quantity

$$K_{\pm} = \exp \left\{ -\mu(z+a) \pm \mu' \int_{-a}^z \frac{dz'}{\{1 + [P - \beta(z')]^2\}^{1/2}} \right\}, \quad (12)$$

where $\mu' = -\text{Im}(\pi/\Lambda)$, and where we have taken photoelectric absorption into account (the absorption coefficient μ). This absorption was omitted along with the inconsequential correction for refraction of the crystal from (2). The two signs in (12) correspond to the first and second terms in (9), respectively. If $|P| \lesssim 1$, the Bloch wave corresponding to the first term in (9) has nodes near the atomic planes and antinodes between them, so that this wave is absorbed anomalously weakly (the Bormann effect), while the wave corresponding to the second term is absorbed anomalously strongly. In the case of strong absorption, the Bloch wave which is subject to the anomalously strong absorption does not reach the exit surface of the crystal, and the image of the defect is determined by the change in the amplitude of the weakly absorbed Bloch wave during interbranch scattering.

Let us assume that the interbranch scattering of the Bloch wave occurs near the $z = 0$ plane and quite far from either surface of the crystal (so that the condition $\mu a \gg 1$ holds). It then follows from (11) that only the wave φ_2 reaches the region of interbranch scattering; in the course of this scattering, this wave generates a wave φ_1 , and the amplitude of the wave φ_2 correspondingly decreases. The wave φ_1 is absorbed over distances on the order of $(2\mu)^{-1}$, and the image is then determined by the amplitude of the wave φ_2 . The interbranch scattering is set by the factor $(1 - \tilde{J}_2)$. The corresponding contribution to the intensity of the diffracted wave is, within terms quadratic in $w'/2\gamma^2$, $|1 - \tilde{J}_2|^2 = 1 - |J_1|^2$. In particular, in the case $\beta(z) = \beta(-z)$ we find

$$|E_1|^2 = |\Gamma_+(-a)\Gamma_-(z)K_+|^2 \times \left\{ 1 - \left| \int_0^{\infty} \frac{w'(z)}{1+w^2(z)} \sin[2(\Phi(z) - \Phi(0))] dz \right|^2 \right\}. \quad (13)$$

Let us examine in more detail the interbranch scattering of Bloch waves in the strain field of a dislocation parallel to the reflection vector. The component of the displacement field parallel to \mathbf{g} , u_x , is determined by the screw component b_x of the Burgers vector:

$$u_x = \frac{b_x}{2\pi} \text{arctg} \frac{z}{y}, \quad (14)$$

where y is the distance from the dislocation line to the scattering plane. According to (6), this component of the displacement field describes the local deviation of the crystal from the Bragg condition,

$$\beta(z) = \frac{\mathbf{g}\mathbf{b}}{2\pi} \frac{\Lambda'y}{y^2+z^2}. \quad (15)$$

The components of the displacement field orthogonal to \mathbf{g} , u_y and u_z , do not contribute to the scalar product $\mathbf{g}\mathbf{u}$ and thus do not cause an effective disorientation of the crystal.

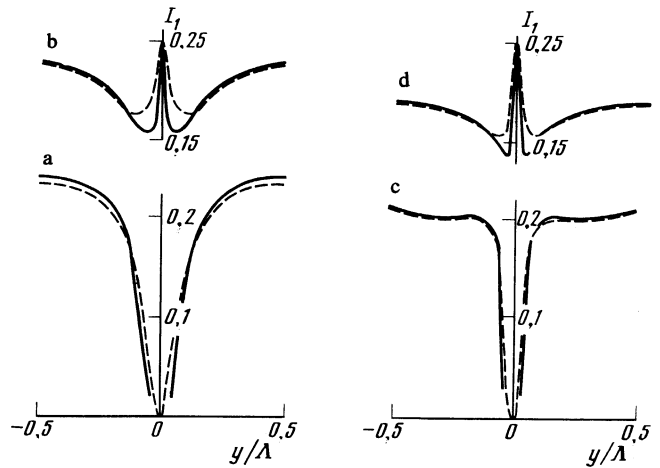


FIG. 1. Image of a dislocation in the case of strong absorption. The absorption coefficient is $\mu = 0.1\pi$; the crystal thickness is 8Λ ; and the Bragg condition is satisfied exactly ($P = 0$). Solid curve—approximation (13); dashed curve—numerical solution of Eqs. (4). a) $\mathbf{g}\cdot\mathbf{b} = 1$; b) $\mathbf{g}\cdot\mathbf{b} = 2$; c) $\mathbf{g}\cdot\mathbf{b} = 3$; d) $\mathbf{g}\cdot\mathbf{b} = 4$.

With decreasing y , the gradient of the effective disorientation w' progressively increases. Straightforward calculations show that the interbranch scattering becomes important at $y \lesssim 0.2\Lambda$. In the limit $y \rightarrow 0$ we have $\beta(z) = 1/2\mathbf{g}\cdot\mathbf{b}\Lambda^{-1}\delta(z)$, corresponding to a stacking fault with a phase shift $2\pi\mathbf{g}\cdot\Delta\mathbf{u} = \pi\mathbf{g}\cdot\mathbf{b}$. If $\mathbf{g}\cdot\mathbf{b}$ is even, the phase shift is a multiple of 2π and corresponds to a displacement of the reflecting planes by an integer number of periods. The free propagation of the Bloch waves is not disturbed. Odd values of $\mathbf{g}\cdot\mathbf{b}$ correspond to a displacement of the reflecting planes by half the period; the Bloch wave which is weakly absorbed in one part of the crystal becomes absorbed in another part, and in the case of strong absorption the intensity of the Bloch wave transmitted through a stacking fault drops to zero.

Figure 1 compares the results calculated on interbranch scattering in approximation (13) with the results of a numerical solution of Eqs. (4) for various values of the diffracting capability of the dislocation $\mathbf{g}\cdot\mathbf{b}$. Approximation (13) gives a good description of interbranch scattering in those regions where this scattering is not strong. For even values of $\mathbf{g}\cdot\mathbf{b}$, expression (13) also gives the correct value at $y = 0$, so that this approximation is a good interpolation over the entire range of y .

Al'shitz *et al.*¹¹ have carried out numerical calculations which reveal the contribution of interbranch scattering and absorption. They proposed a different approximate description of the interbranch scattering, by retaining one of the two terms in (9) and using it to construct another, linearly independent, solution. Chukhovskii *et al.*¹³ have developed an approximate description of interbranch scattering through an expansion in the small parameter $2\pi(1+P^2)^{1/2}y/\Lambda \ll 1$. This approximation describes interbranch scattering only at extremely small values of y . It is also possible to construct a description of interbranch scattering for small y which is analogous to (11), by using as a zeroth approximation the exact solution for a stacking fault (with a phase shift $\pi\mathbf{g}\cdot\mathbf{b}$) instead of the unperturbed Bloch waves. According to Ref. 14, it is the interbranch scattering shown in Fig. 1, rather

than the change in the absorption in the highly distorted region and the repulsion of the Bloch-wave trajectories from this region (for which corresponding calculations were carried out in Ref. 4, for example), which determines the x-ray image of dislocations in the case of the anomalous transmission of one of the two Bloch waves. Absorption is of minor importance here because of the small dimensions of the region which absorbs both of the Bloch waves.

3. INTERBRANCH SCATTERING OF BLOCH WAVES; STRONG DISTORTION FIELDS

We will consider separately the scattering of Bloch waves in the strain field of a dislocation in the case of large values of $\mathbf{g} \cdot \mathbf{b}$, since in this case we cannot use perturbation theory, and the large dimensions of the strong-distortion region present new opportunities for studying the diffraction optics of Bloch waves. Experimental results for this case have been obtained by making use of large reflection orders and a group of closely spaced dislocations; these experimental results are described in Section 5 below (see also Ref. 15). Simple estimates from the condition $\Lambda w' \ll 2\gamma^2$ show that the range of applicability of the eikonal approximation, (9), depends strongly on the value of P . If $|P| \lesssim 1$, then in a region of a high gradient of the effective disorientation, $w' \gg 1$, the effective disorientation w itself will also be large. As a result, approximation (9) is valid for $y \gtrsim (0.2-0.3)\Lambda$. If, on the other hand, $|P| \gg 1$, then approximation (9) can no longer be used at much higher values of y : The crystal disorientation β caused by a dislocation offsets the initial deviation of the wave from the Bragg condition, P , and in the region of large values of w' the value of w may be small.

At small values of y , the diffraction of Bloch waves reduces to an interbranch scattering involving a reversal of the x component of the quasimomentum. As a result, the short-range field of the dislocation serves as a diffraction lens which focuses the Bloch waves.¹⁵

Let us examine the case $|P| \gg 1$ in more detail, since in constructing the Riemann function of a point source for a crystal with a dislocation (in Section 4) we will need to sum the contributions of Bloch waves with all values of P . In regions with $|w| \gg 1$ (in particular, far from the dislocation), the eikonal approximation can still be used. One of the coefficients $\Gamma_{\pm}(z)$ in (9) vanishes, while the other becomes unity, so that the Bloch waves of two families reduce to the waves E_0 and E_1 . It follows from (9) that the wave amplitudes are constant at $|w| \gg 1$, while their phases vary in accordance with

$$E_0 \propto \exp[i\Phi(z) \operatorname{sign} w], \quad E_1 \propto \exp[-i\Phi(z) \operatorname{sign} w], \quad (16)$$

where $\operatorname{sign} w$ is the sign function. Near the dislocation, with $y \lesssim \Lambda$, the maximum disorientation of the crystal (for a given value of y), $\beta(0)$, is much greater than unity. If the momentum satisfies $P \lesssim \beta(0)$, then there are regions in which we have $|w| \lesssim 1$ and thus $\Lambda |w'|/2\gamma^2 \gtrsim 1$. In the strain field of a dislocation there are two such regions, around the points $\pm z_P$ [z_P is the positive root of the equation $\beta(z) = P$]. The eikonal approximation cannot be used there, so that the Bloch-wave amplitudes corresponding to the asymptotic be-

havior of the wave field before and after this region are different. At $z < -z_P$ the amplitudes of the Bloch waves are determined by boundary conditions (5):

$$E_0 = \exp[i\Phi(z) - i\Phi(-a)], \quad E_1 = 0. \quad (17)$$

Near the point $-z_P$, the solution of wave equations (4) does not reduce to two noninteracting Bloch waves (the quasiparticles interact strongly), while at $z > -z_P$ the solution should have the following form, according to (16):

$$\begin{aligned} E_0 &= f_0 \exp\{i[\Phi(-z_P) - \Phi(-a)] - i[\Phi(z) - \Phi(-z_P)]\}, \\ E_1 &= f_1 \exp\{i[\Phi(-z_P) - \Phi(-a)] + i[\Phi(z) - \Phi(-z_P)]\}. \end{aligned} \quad (18)$$

In terms of Bloch waves, the switch from (17) to (18) means that the interbranch scattering has caused a Bloch wave of unit amplitude to create a new Bloch wave with an amplitude $|f_1|$ while suffering a decrease in its own amplitude to $|f_0|$. Energy conservation requires $|f_0|^2 + |f_1|^2 = 1$ (the absorption is slight here because of the small dimensions of the regions of interbranch scattering. The problem of interbranch scattering thus reduces to one of determining the complex scattering amplitudes f_0 and f_1 for the given disorientation $w(z)$. The interbranch scattering must be examined in two regions in the strain field of the dislocation.

We turn now to a determination of the scattering amplitudes. If the disorientation w changes quite rapidly ($\Lambda |w'| \gg 1$), i.e., if the dynamic-diffraction region is narrow ($\Delta z \ll \Lambda$), then we need consider only the energy transfer from the transmitted wave to the diffracted wave (we can ignore the reaction of the diffracted wave on the transmitted wave). This approximation is equivalent to the kinematic approximation (the first Born approximation) and corresponds to the following replacement of the matrix of system (4):

$$\begin{pmatrix} -w & 1 \\ 1 & w \end{pmatrix} \rightarrow \begin{pmatrix} -w & 0 \\ 1 & w \end{pmatrix}. \quad (19)$$

After this simplification, system (4) can easily be solved:

$$\begin{aligned} E_1(z) &= -i \frac{\pi}{\Lambda} \exp\{i\pi[\mathbf{g}\mathbf{u}(z) + \mathbf{g}\mathbf{u}(-a)]\} \\ &\quad \times \int_{-a}^z \exp\left\{2\pi i \left[P \frac{z}{\Lambda} - \mathbf{g}\mathbf{u}(z) \right]\right\} dz. \end{aligned} \quad (20)$$

Since we have $\Lambda |w'| \gg 1$ by assumption, the integral can be evaluated by the stationary-phase method. In particular, for a dislocation in the median plane of the crystal we find

$$E_1(a) = -i \frac{2\pi}{\gamma_P^{1/2}} \sin \left[2\pi \mathbf{g}\mathbf{u}(z_P) - \frac{2\pi}{\Lambda} P z_P + \frac{\pi}{4} \right]. \quad (21)$$

Here $\gamma_P = -\Lambda d\beta/dz|_{z=z_P}$, and the two stationary points $z = \pm z_P$ correspond to the two regions where Bloch waves are created. In the kinematic limit, $|w| \gg 1$, the quantity $(1 + w^2)^{1/2}$ becomes $|w|$, and the phase-change law (10) reduces to the kinematic law (21) [see Eq. (26) below]. Examining the contributions of the stationary points $\pm z_P$ separately, we find the following result for the scattering amplitudes (18):

$$f_0 = 1, \quad f_1 = \frac{\pi}{\gamma_P^{1/2}} \exp\left(-i \frac{\pi}{4}\right). \quad (22)$$

The condition for the applicability of the kinematic approximation is that the amplitude of the diffracted wave, $|f_1|$, be small in comparison with the amplitude of the incident wave; from this condition we find $\gamma_P \gg \pi^2$. Kinematic approximation (19) is thus valid when the dynamic-diffraction region, with $|w| \lesssim 1$, has dimensions less than a tenth of the extinction length Λ .

To find an approximation which holds for $\gamma_P \sim 1$ we note that near the points $\pm z_P$ the function $\beta(z)$ is approximately linear; the region of linearity can be shown by simple calculations to span the entire dynamic-diffraction region, $|w| \lesssim 1$. The solution of system (4) for the linear function $w(z)$ (corresponding to a bending of the crystal) can be expressed in terms of the parabolic cylinder functions (Weber functions). Chukhovskii¹⁶ has derived an exact solution of boundary-value problem (4), (5) and has carried out the necessary expansion of the Weber function for the field $w(z) = \gamma(z - z_0)/\Lambda$ in the strong-bending case ($\gamma \gtrsim 1$), of interest here. The region of interbranch scattering surrounds the point z_0 ; the Bloch waves on the two sides of this region are as described by (17) and (18); and the scattering amplitudes are found to be

$$f_0 = e^{-\pi^2/2|\gamma|}, \quad f_1 = (1 - e^{-\pi^2/|\gamma|})^{1/2} e^{i\delta_g(\gamma)}, \quad (23)$$

where the scattering phase shift δ_g is expressed in terms of the logarithm of the gamma function,

$$\delta_g(\gamma) = -\frac{\pi}{4} + \text{Im} \ln \Gamma\left(1 - i\frac{\pi}{2\gamma}\right) - \frac{\pi}{2\gamma} \ln \frac{\pi}{2\gamma} \quad (24)$$

with $\gamma > 0$ and $\delta_g(-\gamma) = \pi - \delta_g(\gamma)$. Balibar *et al.*¹² have worked from a numerical simulation to construct the wave field in a bent crystal for actually visualizing the trajectory of Bloch waves. They found that after passage through the dynamic region the intensity of the transmitted wave decreases in accordance with $\exp(-\tau/\tilde{\gamma})$, where the bending parameter $\tilde{\gamma}$ is related to our dimensionless parameter γ by $\tilde{\gamma} = \gamma \cos \theta / \Lambda$. The constant τ was found from the numerical simulation to be $\tau = 0.29 \mu\text{m}^{-1}$. The same intensity decay law follows from (23), and for the parameter τ we find simply $\tau = \pi^2 \cos \theta / \Lambda$, which yields $\tau = 0.28 \mu\text{m}^{-1}$ for the conditions of the numerical simulation of Ref. 12. (More recently, this problem has been studied analytically.¹⁷) In the two regions of dynamic diffraction in the strain field of the dislocation, $z = \mp z_P$, we must use Eqs. (23) with the bending-parameter values $\gamma = \pm \gamma_P$. It is easy to see that at $\gamma_P \gg \pi^2$ the results of the dynamic theory, (23), convert to the kinematic limit, (22). Applying Eqs. (23) twice, we find the following results for the amplitude of the diffracted wave in the $z = a$ plane:

$$E_1(a) = -2i \left(1 - e^{-\frac{\pi^2}{\gamma_P}}\right)^{1/2} e^{-\frac{\pi^2}{2\gamma_P}} \sin[\Phi(z_P) - \Phi(-z_P) - \delta_g(\gamma_P)]. \quad (25)$$

Since w is much greater than unity for nearly all values of z , $(1 + w^2)^{1/2}$ becomes $|w|$; the phase change law becomes the kinematic law,

$$\Phi(z_P) - \Phi(-z_P) \approx \frac{\pi}{\Lambda'} \int_{-z_P}^{z_P} |\beta(z') - P| dz' = 2\pi \text{gu}(z_P) - \frac{2\pi}{\Lambda'} P z_P; \quad (26)$$

and Eq. (25) becomes (21) with $\gamma_P \gg \pi^2$. With decreasing γ_P , the amplitude of the diffracted wave in the kinematic approximation, (21), increases and can become greater than unity, since energy is not conserved in the kinematic approximation, (19), while in approximation (25) the amplitude of the diffracted wave is never greater than unity.

4. RIEMANN FUNCTION FOR A CRYSTAL WITH A DISLOCATION

The results derived above can be tested directly in experiments on the diffraction of x-ray plane waves: The changes in the wave fields over depth can be followed by using a wedge-shaped crystal. Of more interest for problems of dynamic diffraction in a crystal with a dislocation, however, is the Riemann function (influence function) describing the propagation of a perturbation from a point source. The Riemann function can be used to construct the solution of an arbitrary spatially inhomogeneous problem,¹ and the Riemann function itself can be observed experimentally by means of topographic sections when the x-ray wave is incident on the crystal through a narrow slit on the surface (the width of the slit must be much smaller than the extinction length). Since the slit width is much smaller than the distances over which the amplitudes E_0 and E_1 change in Eqs. (2), the boundary conditions on these equations at the entrance surface ($z = -a$) of the crystal can be written in the following form:

$$E_0|_{z=-a} = \delta(x), \quad E_1|_{z=-a} = 0. \quad (27)$$

As we have already mentioned, the Riemann function is known exactly in extremely few cases: for an ideal crystal,¹ for a uniformly bent crystal,⁶ and for a crystal with a stacking fault.⁷ We would like to determine the Riemann function approximately for a crystal with a dislocation. For this purpose we expand the plane wave incident on the crystal through a narrow slit in plane waves,

$$\delta(x) = \frac{\text{ctg} \theta}{2\Lambda'} \int_{-\infty}^{\infty} \exp\left(i\frac{\pi}{\Lambda'} Px \text{ctg} \theta\right) dP, \quad (28)$$

and we sum the solutions derived above for the plane-wave problems, $E_i(z; P, y)$:

$$E_1(x, y, z) = \frac{\text{ctg} \theta}{2\Lambda'} \int_{-\infty}^{\infty} E_1(z; P, y) \exp\left(i\frac{\pi}{\Lambda'} Px \text{ctg} \theta\right) dP. \quad (29)$$

At sufficiently large values of y we can use the eikonal approximation (9). Fourier transformation (29) can be carried out by the stationary-phase method (cf. Ref. 18). The stationary-phase condition

$$x \text{ctg} \theta = \mp \int_{-a}^z \frac{P - \beta}{(1 + (P - \beta)^2)^{1/2}} dz \quad (30)$$

determines the trajectory of a Bloch wave with a generalized momentum P which remains constant along the trajectory. The amplitude of the diffracted wave is found to be

$$E_1 = A_+ K_+ e^{iS_+} + A_- K_- e^{iS_-}. \quad (31)$$

The phase shift of the wave along the trajectory is given by

$$S^\pm = \frac{\pi}{\Lambda'} \left[\pm \int_{-a}^z (1 + (P - \beta)^2)^{1/2} dz + Px \operatorname{ctg} \theta \right] - \frac{\pi}{2} \mp \frac{\pi}{4}, \quad (32)$$

and the amplitude factors are

$$A_\pm = \frac{\operatorname{ctg} \theta}{2\Lambda'} \Gamma_\pm(-a) \Gamma_\mp(z) (2\pi/\Phi'')^{1/2}, \quad (33)$$

where

$$\Phi'' = \frac{\partial^2 \Phi}{\partial P^2} = \frac{\pi}{\Lambda'} \int_{-a}^z \frac{dz}{[1 + (P - \beta)^2]^{3/2}}. \quad (34)$$

The upper and lower signs in (30)–(33) refer to the weakly and strongly absorbed waves, respectively. Equations (12) and (30)–(33) parametrically determine $E_1(x, y, z)$ and constitute the solution of the equations of x-ray geometric optics^{1,2} for the field $w = w(z)$. In the geometric-optics approximation, the propagation of a Bloch wave in a distorted crystal is analogous to the motion of a relativistic particle in an external field: The weakly and strongly absorbed Bloch waves correspond to particles with masses of opposite signs; the coordinate z plays the role of the energy; and the disorientation β plays the role of the external electric potential. In our problem the coordinate x is cyclic, (15), so that the momentum P is conserved, and the geometric-optics equations can be integrated.⁸

For solving the plane-wave problem it was sufficient to examine the interference of two Bloch waves, (9), corresponding to two sheets of the dynamic dispersion surface. Now, the narrow slit on the surface of the crystal acts as a source of an entire beam of Bloch-wave trajectories; we must follow trajectories (30) of two families of rays, find two rays from different families which pass through the same point (x, y, z) , and calculate their phase difference, (32). It is this phase difference which determines the interference pattern of the image. A detailed quantitative comparison of the eikonal surfaces $S^\pm(x, y)$ with the position and shape of the interference fringes was carried out for dislocation field (15) in Refs. 8 and 19. If $\mathbf{g} \cdot \mathbf{b}$ amounts to a few units, the entire interference pattern of the image can be described in the ray approximation. An exceptional case is the region $y \rightarrow 0$, where, as was shown in Ref. 15, there is a focusing of Bloch waves analogous to the focusing by a stacking fault.⁷

In strong distortion fields (at large values of $\mathbf{g} \cdot \mathbf{b}$) we find a completely different situation: Interbranch scattering becomes important over a broad range of y , and a “central image” generated by interbranch scattering appears on the topographic sections (see Section 5 and Ref. 15). Let us examine the corresponding contribution to the Riemann function in more detail. The fine structure of this central image makes it possible to unambiguously determine the diffraction mechanism involved in the image formation.

As was shown in Section 3, for Bloch waves with generalized momenta $P \lesssim 1$ approximation (9) remains valid. The Fourier transformation (29) again leads to expressions (30)–(34). The additional contribution to the Riemann function is due entirely to the interbranch scattering of Bloch waves with momenta $P \gg 1$. To determine this contribution, we use the approximations derived in Section 3.

Fourier transformation (29) in the kinematic approxi-

mation, (20), can easily be carried out because of the δ function $\delta(z' + 1/2x \cot \theta)$ which arises in the integration over P . This δ function has a simple physical meaning: In this approximation, the new wave E_1 is transported, without any further diffraction, along the direction (s_1) of the diffracted wave; the value $z' = -(x \cot \theta)/2$ corresponds to the creation point for the wave which arrives at the point with coordinate x in the $z = a$ plane. In this approximation, the wave E_1 directly conveys the displacement field \mathbf{u} at the point at which it was created:

$$E_1(a) = -i \frac{\operatorname{ctg} \theta}{4\Lambda'} e^{-2\mu a} \exp \left[-2\pi i \mathbf{g} \cdot \mathbf{u} \left(-\frac{x \operatorname{ctg} \theta}{2} \right) \right]. \quad (35)$$

This result can be derived directly, without appealing to the Fourier representation, by relating the wave field which is created to the strain field of the distortions near the dislocation, as discussed in Ref. 20. We restrict the discussion here to the waves in the $z = a$ plane, since the subsequent propagation of the wave E_1 is simply a parallel transport along the s_1 direction.

The inverse Fourier transformation of expression (25) can be carried out by the stationary-phase method. Since (25) describes Bloch waves with momenta $P \gg 1$, their trajectories (30) are straight lines along the direction of the characteristic s_1 , by virtue of the condition $w \gg 1$. The stationary condition reduces to $z_p = 1/2|x| \cot \theta$ and determines that Bloch-wave momentum P for which the region of interbranch scattering lies at a value of z such that, during the subsequent propagation along the s_1 direction, the new Bloch wave arrives at the point x in the $z = a$ plane. By virtue of (26), the phase of the wave E_1 in this approximation differs only slightly from the phase in kinematic approximation (35). We will not write out the corresponding corrections here. The

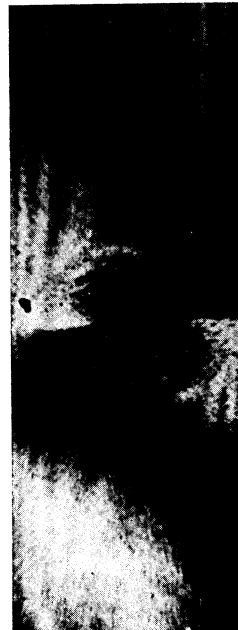


FIG. 2. Topographic section with an image of four closely spaced screw dislocations (the distance between dislocations is $\approx 2\text{--}5 \mu\text{m}$). Crystal thickness of $410 \mu\text{m}$; Mo $K\alpha$ radiation; (660) reflection; dislocation axis parallel to the [110] direction; $1/2[110]$ Burgers vector for each dislocation; (111) surface of the crystal.

amplitude (25) leads to the appearance in (35) of an amplitude factor

$$\frac{\gamma_P^{1/2}}{\pi} (1 - e^{-\pi^2/\gamma_P})^{1/2} e^{-\pi^2/2\gamma_P}, \quad (36)$$

where the value of P is found from the condition $z_p = 1/2|x|\cot\theta$. At $\gamma_P \gg \pi^2$, the quantity in (36) becomes equal to unity, as it should. With increasing $|x|$ and thus with decreasing P , the quantity in (36) falls off exponentially, leading to the finite "width" in the x direction of the packet of new Bloch waves. [In the limit $x \rightarrow 0$ we must take into account the creation of Bloch waves at small values of z , where the function $\beta(z)$ is very nonlinear; expressions (23) cannot be used for the scattering amplitudes in this region.]

Since the packet of newly created Bloch waves consists of waves with momenta $P \gg 1$, during the subsequent propagation through the crystal along trajectories (30) this packet undergoes almost no deviation from the s_1 direction and is transported in this direction, undergoing nearly no broadening and retaining its structure (see Fig. 3 below).

5. FORMATION OF THE DISLOCATION IMAGE

Figure 2 shows an x-ray topographic section of a group of four closely spaced screw dislocations with a resultant Burgers vector $\mathbf{b} = a_0[2\bar{2}0]$, oriented parallel to the reflection vector (see also Ref. 15, where a systematic experimental study was made of the images of isolated screw dislocations, isolated 60° dislocations, and groups of dislocations). Since we have $\mathbf{g} = a_0^{-1}[\bar{6}60]$, the diffraction capability of the dislocations in Fig. 2 is $\mathbf{g} \cdot \mathbf{b} = 24$. The progressive change in the shape of the extinction contours as the dislocation is approached has been analyzed in detail previously^{8,19} in the geometric-optics approximation. We can accordingly focus our attention on the central part of the image, where we see the effects of the diffraction optics of Bloch waves. The particular way in which the image depends on the absorption and the behavior of the waves in the crystal can be determined not simply from experiments but also by means of numerical simulations. Figure 3 shows topographic sections and the intensity distribution of the diffracted wave in the scattering plane according to calculations from Takagi's equations, (2),

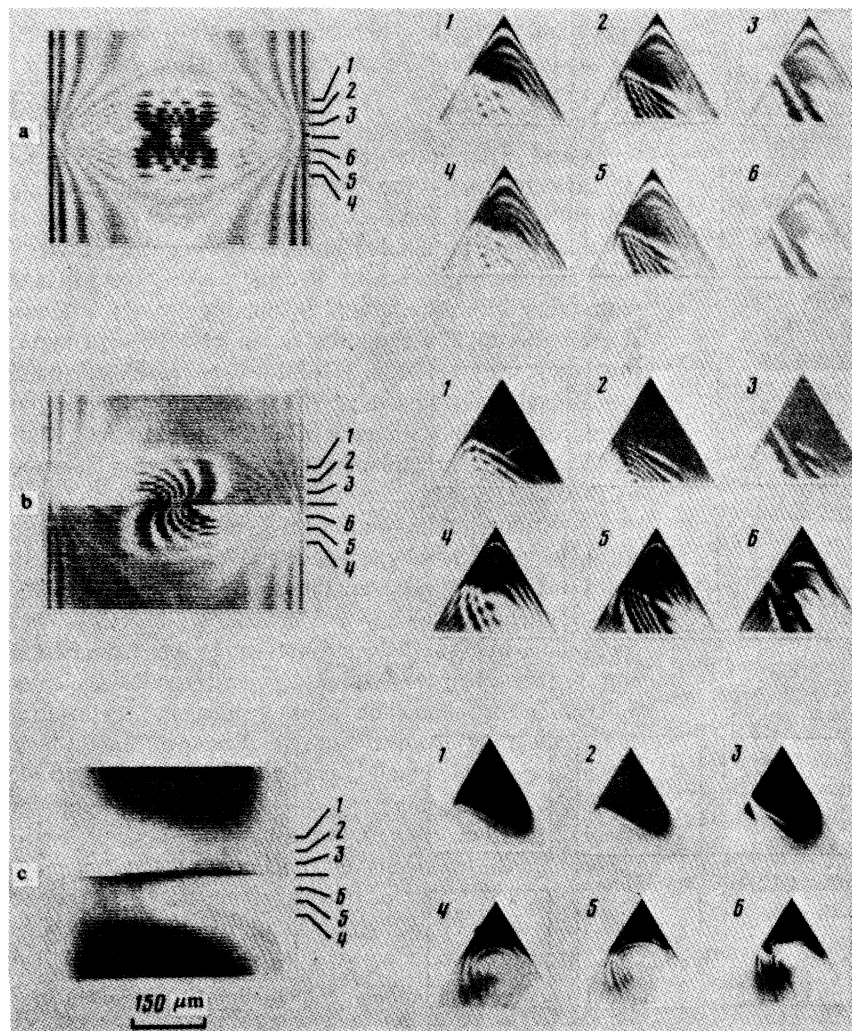


FIG. 3. Calculated topographic sections corresponding to the experimental results shown in Fig. 4; distribution of the intensity of the diffracted wave in the crystal. a— $\mu t = 0$; b— $\mu t = 3$; c— $\mu t = 12$.

for various values of the absorption coefficient μ (the values of the other parameters correspond to the experiments shown in Fig. 2). The algorithm of Ref. 21 was used for the numerical solution of Takagi's equations, and the blackening scale proposed in Ref. 2 was used for visualizing the images with the computer printer. In the absence of absorption (Fig. 3a) the central image is symmetric with respect to the x and y axes of the topographic section and consists of two families of interference fringes, while the distribution of the diffracted wave in the scattering planes is the same on the two sides of the dislocation. When μt is a few units (Fig. 3b), corresponding to the experimental conditions, we are left with only a single family of fringes, and we see an asymmetry of the intensity distribution in the Borrmann triangle on both sides of the dislocation. The good agreement of the experimental (Fig. 2) and calculated (Fig. 3b) sections justifies the replacement of the group of closely spaced dislocations by a single superdislocation. At $\mu t \gg 1$ (Fig. 3c), the central image loses its interference nature, but the symmetry remains the same.

The analysis of Section 4 makes it possible to completely describe the image formation as a function of the absorption level. In that section we expanded the wave packet incident on the crystal through a narrow slit in plane waves, with all possible values of the deviation from the Bragg condition, P , and we followed the motion of the Bloch waves created by this packet in the crystal. Two families of Bloch waves with momenta $P \lesssim 1$ propagate along trajectories (30). The waves with momenta $P \gg 1$ undergo almost no diffraction in the crystal and propagate along the direction (s_0) of the incident wave until they reach the highly disoriented region near the dislocation, where the Bragg condition is satisfied locally for these waves ($w = 0$). Interbranch scattering occurs there, and new Bloch waves are created. They propagate along the s_1 direction. If there is no absorption (Fig. 3a) the image is determined by the interference of three families of Bloch waves: the two families which have undergone refraction and the new family created upon the diffraction of the Bloch waves. In accordance with the symmetry properties established in Section 1, the intensity distribution in the crystal is symmetric with respect to the xz plane, while in the $z = a$ plane the topographic section is also symmetric with respect to the x and y axes. The basic features of the image remain the same when there is absorption (Fig. 3b). In this case the strongly absorbed Bloch waves, for which the absorption coefficient is approximately 2μ according to (12), do not reach the exit surface of the crystal, and the contrast is determined by the interference of the weakly absorbed Bloch waves [the first term in (31)] with the Bloch waves created during the interbranch scattering, (35). According to (31) and (35), the intensity maxima in the interference pattern occur at the positions determined by the condition

$$S^+(x) + \left[2\pi g u \left(-\frac{x \operatorname{ctg} \theta}{2} \right) + \frac{\pi}{2} \right] = 2\pi n, \quad (37)$$

where n is an integer. Figure 4 is a contour map of the phase difference (37) in the (x, y) plane of the topographic section at $z = a$. As follows from (14), the family of curves of constant value of the wave phase (35) constitute a fan of straight lines

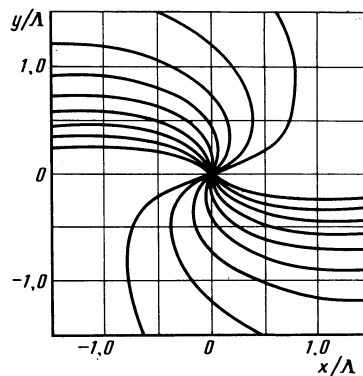


FIG. 4. Shape of the interference fringes on the image of a dislocation according to calculations from Eq. (37) (cf. Figs. 2 and 3b).

which emerge from the origin. A slight x dependence of the phase S^+ changes the packing density of these lines, while a y dependence of S^+ causes the lines of a constant phase difference to become curved. In the $z = a$ plane, the image is centrally symmetric.

The good agreement in terms of the number, position, and shape of the contour lines in Fig. 4, on the one hand, and Figs. 2 and 3b, on the other, supports our arguments regarding the mechanisms for the image formation and confirms the calculations of the wave amplitudes and phases on the basis of these mechanisms. The phase of the wave created in the course of the interbranch scattering in approximation (35) directly conveys the displacement field u in the strong-distortion region. The slowly varying wave (31) is a sort of reference wave for a holographic recording of this information, and the displacement field $u(r)$ can be reconstructed from the interference pattern by making use of the known⁸ reference beam, as was pointed out in Ref. 20. With increasing x or y , the amplitude (36) of the wave created during the interbranch scattering falls off exponentially, determining the dimensions of the region of the "central image" (about 3Λ in our case). Outside this region, the image is determined by Bloch waves (31).

Pendulum oscillations of the intensity of the diffracted wave, which create hyperbolic interference fringes in the scattering plane (Fig. 3), are determined by the interference of two Bloch waves (31) which have undergone refraction in the strain field of the dislocation. It can be seen from Figs. 3b and 3c that when there is absorption the contrast is very different in the sections on different sides of the dislocation. This effect is analogous to those which arise during the bending of an absorbing crystal, when the ratio of the amplitudes of the two Bloch waves and the contrast of the pendulum fringes depend on the sign of the curvature of the reflecting planes.²³ In the highly distorted region, the excitation points shift toward the edge of the dispersion curve, so that the directions of the Poynting vectors approach the directions of the transmitted wave (s_0) and the diffracted wave (s_1). At $y > 0$, the weakly absorbed wave propagates along the s_0 direction in the strong-distortion region, while the strongly absorbed wave propagates along the s_1 direction. Nearly all the energy of the weakly absorbed Bloch wave is in the wave E_0 , while nearly all the energy of the strongly absorbed wave

is in E_1 . Working from the condition $w \gg 1$, (7), and (33), we can easily find the ratio of the amplitude factors, $A_+ \ll A_-$. Although the absorption of the Bloch waves is different, and we have $K_+ \gg K_-$, the amplitudes of these Bloch waves in the wave E_1 are comparable ($A_+ K_+ \sim A_- K_-$), and (31) determines the interference contrast. At $y < 0$, the effective disorientation w changes sign; the excitation points shift toward the other edge of the dispersion surface; and we find the opposite ratio of amplitude factors, $A_+ \gg A_-$. Since the relation $K_+ \gg K_-$ still holds, we find $A_+ K_+ \gg A_- K_-$, explaining why there is no interference contrast. After the region of strong distortions is crossed, the excitation points return to their original positions, and the amplitude factors become comparable ($A_+ \sim A_-$). Since $K_+ \gg K_-$, the condition $A_+ K_+ \gg A_- K_-$ holds outside the strong-distortion region, regardless of the sign of y , and there is no interference contrast due to the interference of the two families of Bloch waves which have undergone refraction.

The slight difference in curvature of the interference contours on the experimental (Fig. 2) and calculated (Fig. 3b) topographic sections can be attributed to an anisotropy of the crystal (ignored in the computer calculations). Under our experimental conditions, with the x axis being a twofold axis and the z axis a threefold axis, the anisotropy leads to the replacement of the displacement components u_x , (14), by

$$u_x = \frac{b_x}{2\pi} \operatorname{arctg} \frac{\nu z}{y}, \quad (38)$$

according to Ref. 24, where $\nu = (c'_{55}/c'_{44})^{1/2} = [(A + 2)/(2A + 1)]^{1/2}$, and $A = 2c_{44}/(c_{11} - c_{12})$ is an anisotropy parameter ($\nu = 0.91$ for silicon). Comparison of (14) and (38) reveals that taking the anisotropy into account reduces to changing the scale along the y axis by a factor of ν . After this change of scale, we find a quantitative agreement between the curvature of the contours on the experimental and calculated topographic sections.

In the case $\mu t \gg 1$ (Fig. 3c), neither the strongly absorbed Bloch wave nor the wave (35), which undergoes a normal absorption, reaches the exit surface of the crystal. The contrast is determined by the intensity of the weakly absorbed wave in (31):

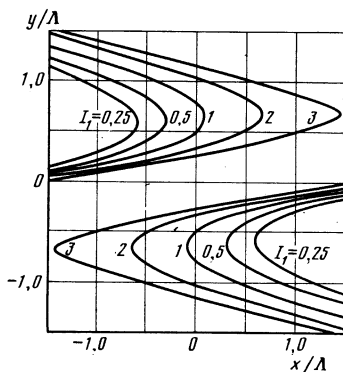


FIG. 5. Amplitude contrast of an image of a dislocation in the case of strong absorption ($\mu t = 12$), according to calculations from Eq. (38) (cf. Fig. 3c).

$$|E_1(a, x)|^2 = \left| \left[\frac{\operatorname{ctg} \theta}{2\Lambda'} \Gamma_+(-a) \Gamma_-(a) \right] K_+ \left(\frac{2\pi}{\Phi''} \right)^{1/2} \right|^2. \quad (39)$$

The three factors here determine, respectively, the amplitude E_1 in the Bloch wave which arise at the point x , according to (30); the absorption of the Bloch wave along its trajectory; and the change in the packing density of the trajectories. Figure 5 shows curves of constant intensity determined parametrically by Eqs. (39) and (30).

The validity of our determination of the image-formation mechanism in the case of strong absorption is confirmed by the good agreement of Fig. 5 and Fig. 3c and also of the experimental x-ray topographic section found for the same sample as for the section in Fig. 2, through the use of $\text{Cu } K\alpha$ radiation. With increasing absorption, the interference image on the section fades, but the asymmetry of the image on the two sides of the dislocation remains (cf. Fig. 3c and Fig. 5), making it possible to determine the sign of the Burgers vector of the dislocation.

In summary, the differences in the absorption of the three families of Bloch waves cause the mechanism for the image formation to change with increasing absorption. It thus ultimately becomes possible to determine the contributions of each of the families of Bloch waves to the image.

- ¹V. L. Indenbom and F. N. Chukhovskii, Usp. Fiz. Nauk **107**, 229 (1972) [Sov. Phys. Usp. **15**, 298 (1972)].
- ²L. V. Azaroff, R. Karlow, N. Kato, R. J. Weiss, A. J. C. Wilson, and R. A. Young, X-Ray Diffraction, McGraw-Hill, New York, 1974.
- ³E. V. Suvorov, Rentgenovskaya optika blokhovskikh voln v kristallakh s defektami (X-Ray Optics of Bloch Waves in Crystals with Defects; Dissertation), Chernogolovka, 1981.
- ⁴F. N. Chukhovskii and A. A. Shtol'berg, Zh. Eksp. Teor. Fiz. **64**, 1033 (1973) [Sov. Phys. JETP **37**, 525 (1973)].
- ⁵V. L. Indenbom, I. Sh. Slobodetskii, and K. G. Truni, Zh. Eksp. Teor. Fiz. **66**, 1110 (1974) [Sov. Phys. JETP **39**, 542 (1974)].
- ⁶P. V. Petrashev' and F. N. Chukhovskii, Zh. Eksp. Teor. Fiz. **69**, 477 (1975) [Sov. Phys. JETP **42**, 243 (1975)].
- ⁷V. L. Indenbom and I. Sh. Slobodetskii, Phys. Status Solidi **b71**, 751 (1975).
- ⁸V. L. Indenbom, V. I. Nikitenko, E. V. Suvorov, and V. M. Kaganer, Phys. Status Solidi **a46**, 379 (1978).
- ⁹L. D. Landau and E. M. Lifshitz, Élektrodinamika sploshnykh sred, Nauka, Moscow, 1982, Ch. 16 (Electrodynamics of Continuous Media, Pergamon, New York).
- ¹⁰C. J. Ball, Philos. Mag. **9**, 541 (1964).
- ¹¹V. I. Al'shitz, V. L. Indenbom, and I. A. Rusakova, Kristallografiya **22**, 1157 (1977) [Sov. Phys. Crystallogr. **22**, 659 (1977)].
- ¹²F. Balibar, Y. Epelboin, and C. Malgrange, Acta Crystallogr. **A31**, 836 (1975).
- ¹³F. N. Chukhovskii, A. M. Arustamyan, and Z. G. Pinsker, Kristallografiya **24**, 720 (1979) [Sov. Phys. Crystallogr. **24**, 413 (1979)].
- ¹⁴E. V. Suvorov, V. L. Indenbom, O. S. Gorelik, I. A. Rusakova, and V. A. Chamrov, Phys. Status Solidi **a60**, 27 (1980).
- ¹⁵E. V. Suvorov, V. I. Polovinkina, V. I. Nikitenko, and V. L. Indenbom, Phys. Status Solidi **a26**, 385 (1974).
- ¹⁶F. N. Chukhovskii, Metallofizika **2**, 24 (1980).
- ¹⁷F. Balibar, F. N. Chukhovskii, and C. Malgrange, Acta Crystallogr. **A39**, 387 (1983).
- ¹⁸V. L. Indenbom, V. I. Nikitenko, V. I. Polovinkina, E. V. Suvorov, F. N. Chukhovskii, and A. A. Shtolberg, Collected Abstracts, Second European Cryst. Meeting, Keszthely (Hungary), 1974, p. 66.
- ¹⁹E. V. Suvorov, O. S. Gorelik, V. M. Kaganer, and V. L. Indenbom, Phys. Status Solidi **a54**, 29 (1979).
- ²⁰E. V. Suvorov and V. L. Indenbom, 4-ya Mezhdunarodnaya shkola spet-

sialistov po rostu kristallov (Proceedings of the Fourth International School of Crystal-Growth Specialists, Suzdal', 1980), Part II, p. 229.

²¹A. Authier, C. Malgrange, and M. Tournarie, *Acta Crystallogr.* **A24**, 126 (1968).

²²Y. Epelboin and A. Lifchitz, *J. Appl. Crystallogr.* **A25**, 356 (1969).

²³C. Malgrange, *Acta Crystallogr.* **A25**, 356 (1969).

²⁴J. P. Hirth and J. Lothe, *Theory of Dislocations*, McGraw-Hill, New York, 1967 (Russ. transl. Atomizdat, Moscow, 1972, Ch. 13).

Translated by Dave Parsons